An investigation of the structural aspects of the tomato fruit by means of quantitative nuclear magnetic resonance imaging

Maja Musse, Stéphane Quellec, Marie Francoise M. F. Devaux, Mireille Cambert, Marc Lahaye, François Mariette

An Investigation of Structural Aspects of Tomato Fruit by Means of Quantitative Nuclear Magnetic Resonance Imaging

Maja Musse*[1,2], Stéphane Quellec[1,2], Marie-Françoise Devaux[3], Mireille Cambert[1,2], Marc Lahaye[3], François Mariette[1,2]

[1] - Cemagref, Food Process Engineering Research Unit, 17, avenue de Cucillé, F-35044 Rennes Cedex, France

[2] – Université européenne de Bretagne, France.

[3] - UR1268 Biopolymères Interactions Assemblages, INRA, F-44300 Nantes, France

* Corresponding author. Tel: +33 2 23 48 21 79; Fax: +33 2 23 48 21 15

E-mail address: maja.musse@cemagref.fr

ABSTRACT

In this study, Magnetic Resonance Imaging (MRI) was applied to studying the structural aspects of tomato fruit. The main study was performed on tomatoes (cv. Tradiro) using a 0.2 T electromagnet scanner. Spin echo images were acquired to visualize the tomato macrostructure. The air bubble content in tissues was evaluated by exploiting susceptibility effects using multiple gradient echo images. The microstructure was further studied by measuring spin-spin (T_2) and spin-lattice (T_1) relaxation time distributions. In order to emphasis the MRI results, Nuclear Magnetic Resonance (NMR) Relaxometry, macro vision imaging and chemical analysis were used as complementary and independent experimental methods. MRI images showed that the air bubble content varied between tissues. The presence of gas was attested by macro vision images. Quantitative imaging showed that T_2 and T_1 maps obtained by MRI reflected the structural differences between tomato tissues

and made it possible to distinguish between them. The results indicated that cell size and chemical composition contribute to the relaxation mechanism.

Key words: MRI; NMR; plant; tomato; spin-lattice relaxation; spin-spin relaxation; air bubble

INTRODUCTION

Much research has been carried out in the tomato fruit to determine the factors involved in end use quality such sensory texture properties. The texture of fleshy fruit is affected by both the cellular structure and the biochemical composition of the tissue. Tissue organisation, depending on cell morphology, cell arrangement and cell and tissue properties, is also thought to influence the mechanical properties of plants. In this context, MRI can provide indirect or direct information both at the cell and macroscopic levels with the advantage of non-destructive analysis. This is particularly interesting for investigation the aspects such as fruit changes with ripening or disorder developing.

Magnetic Resonance Imaging has been used for non-destructive studying of the internal structures and micro dynamics of water in various fruit and vegetable tissues [1]. Quantitative MRI is particularly suitable for plant investigations as the relaxation times and proton density are known to be strongly related to the microstructure of plant tissues. However, only a few MRI studies of tomato fruit have been reported until now. Saltveit et al [2] used qualitative MRI to investigate the tomato ripening and showed that differences in the maturity can be seen in the images. Ishida et al [3] measured spin-lattice relaxation time (T_1) in a single green and in a single mature tomato fruits and indicated that T_1 of tissues changes between the two ripening stages. Iwahashi et al [4] investigated the heat stress in tomato fruits by qualitative MRI imaging and measured spin-spin relaxation time (T_2) in the pericarp and locular tissues before and after thermal process. Finally, Gonzalez et al [5] used MRI anatomical images to evaluate internal structural changes of tomato during compression. Otherwise, NMR was used to measure T_2 and water diffusion coefficient in the outer pericarp [6]. Despite results of these investigations, any quantitative MRI or NMR study of both T_2 and T_1 relaxation

parameters and proton density of all the tomato fruit tissues has been reported up to now, which prevents a reliable image interpretation. Moreover, to our knowledge, tissue characteristics such as gas bubbles content have not been investigated until now.

The first aim of the present study was to perform a detailed investigation of the tomato fruit structure by means of spatially resolved quantitative measurements of T_2 and T_1 relaxation times and to evaluate the air bubble content by exploiting susceptibility effects in the multiple gradient echo sequences. Our intention was to provide a reference for further investigations of aspects such as tomato ripening or disorder development. The second aim was to investigate physical parameters which influence relaxation processes. NMR Relaxometry was used to measure relaxation times without the corrupting effects of imaging gradients, contributing therefore to understanding their influence on MRI T_1 and T_2 mapping. Macro vision technique, chosen rather than conventional microscopy because of large dimensions of tomato cells, made it possible to correlate the results of the MRI study with cell size and organization and to visualise air bubbles in tissues. Water and sugar contents were measured in the tomato fruit tissues in order to explain the differences in T_2 and T_1 between tissues. The complexity of the interpretation of the MRI image contrast was finally demonstrated on a spin-echo images by taking into account the relaxation times, proton density and air bubble distributions.

MATERIALS AND METHODS

Tomatoes

Nineteen Tradiro tomatoes provided by the Ctifl (Centre Technique Interprofessionel des Fruits et Légumes, France) were used in this study. Fruit were picked at late green stage (tomato colour code 3-4, Ctifl, France) and stored in a constantly aerated ripening chamber under controlled conditions (18°C and 55%RH) for 9 days. All MRI, NMR macro vision experiments and water content measurements were performed on the same day at the end of this period. The tomatoes were then red, firm and without any external defects.

Magnetic Resonance Imaging

Image acquisition

Measurements were performed on a 0.2 T MRI scanner (Magnetom Open, Siemens, Erlangen, Germany) equipped with a multipurpose flexible receiver coil (MP_S). The maximum imaging gradients were 15 mT/m along all axes. In order to guarantee a constant temperature (18°C) for the tomatoes during measurements, fruit were positioned in the ripening chamber in a specifically designed experimental thermo-insulated support. The support was closed with a cap for at least half an hour before being placed in the magnet. The temperature of the thermally insulated Faraday cage was also set at 18°C.

The MRI experiments were performed on 9 tomatoes. For each tomato, a spin-echo (SE) "morphological" image of the median equatorial plane was acquired with: echo time (TE)=15 ms, recycle time (TR)=200 ms, matrix size=128² pixels, field of view (FOV)=90² mm², slice thickness =3 mm, 15 averages resulting in a total acquisition time of 6min 40 s.

For the other images the same plane was studied with the following geometrical parameters: matrix size=128² pixels, FOV=128² mm² and slice thickness=5 mm.

Air distribution in the tomatoes was studied from two spoiled gradient echo (GE) images acquired with: flip angle=40°, TR=1 s, 2 averages and TE_1=9 ms and TE_2=40 ms, for the first and second images, respectively, resulting in a total acquisition time of 4 min 18 s.

T_1 relaxation and corresponding signal intensity at equilibrium $M_0(T_1)$ maps were measured using the TOMROP sequence (T One Multiple Read-Out Pulses) [7] on only three of the nine tomatoes studied (because of the long acquisition time). The parameters of the sequence were: TI=210 ms, N_{TI}=32, angle=10°, TR=10 s, 3 averages and acquisition time=1h4min.

T_2 relaxation and corresponding signal intensity at equilibrium $M_0(T_2)$ maps were obtained from multi spin echo sequence (MSE) with: first echo equal to inter-echo spacing TE=30 ms, number of consecutive echoes N=32, TR=10 s, 2 averages and acquisition time=43 min.

Finally, one extra tomato fruit was used to acquire T_2 maps with the same parameters as described below, except for TE which was successively set at 30, 50 and 90 ms. The aim of the latter experiment was to study the effects of echo time spacing on T_2 measurements.

The correction for the non uniformities of the MRI scanner was performed by division of pixels of MR tomato images by the corresponding pixels of the water phantom images. Phantom images were acquired at the same settings as the corresponding tomato images, except the increased number of averages and TR.

The magnitude of the MSE and TOMROP image series was fitted on a pixel-by-pixel basis using corresponding monoexponential functions, via the Levenberg-Marquardt criterion for chi-square minimization implemented on Scilab software. MSE and TOMROP data were fitted with a two-parameter [8] and three-parameter [7] functions, respectively. The standard error maps of each fitted parameter were computed for each T_2 and T_1 map.

Regions of interest (ROI) were drawn manually from the T_2 maps that corresponded to a homogeneous region in each tissue and applied to T_2, $M_0(T_2)$, T_1, $M_0(T_1)$ and GE images. The average intensities and corresponding standard deviations were measured within these regions. The standard deviation for T_2, $M_0(T_2)$, T_1, $M_0(T_1)$ maps included the error of exponential fit and the studied parameter variability inside a given tissue.

NMR Relaxometry

NMR Relaxometry measurements were performed on a 20 MHz (0.47 T) spectrometer (Minispec PC-120, Bruker, Karlsruhe, Germany) equipped with a thermostated probe. T_2 was measured using the Carr-Purcell-Meiboom-Gill (CPMG) sequence: 10000 successive echoes were recorded with a 90°-180° pulse spacing of 1 ms. Data were averaged over eight acquisitions and a recycle delay was adjusted for each sample to avoid saturation. T_1 was measured using a fast saturation recovery sequence (SR). 1000 points were acquired from 30 ms to the recovery delay value of 10s. The total acquisition time of data for T_2 and T_1 computing, including spectrometer adjustments, was about 25 min per sample.

Samples were prepared from the core, placenta and outer pericarp of five tomatoes as follows: a one centimeter thick slice was cut in the equatorial region perpendicular to the pedicle axis, and cylinders (0.8 mm in diameter) were cut into the core, the placenta and the outer pericarp (tissue nomenclature [9] is given on Fig. 1). Samples were wiped to remove

water from the broken cells and then placed in NMR tubes and closed with a cap. Measurements were performed at 18°C once the temperature had stabilized within the sample. While performing measurements on one sample, the other tubes were kept in a thermo-regulated chamber at 18°C and used successively.

NMR T_2 and T_1 relaxation curves were fitted by Scilab software according to two different methods, the maximum entropy method (MEM) [10], which provides a continuous distribution of relaxation components without any assumption concerning their number, and the Levenberg-Marquardt algorithm which allows discrete solution for the fitting curve.

Statistical Analysis

Analysis of variance (ANOVA) was performed on the results of quantitative MRI, NMR and water and sugar content measurements using the software package Statgraphics Plus (Centurion) to detect significant differences between tomato tissues (P=0.05 level). When differences between tomato tissues were detected, the multiple range Fisher LSD (Least Significant Difference) test was performed. As the most commonly unacceptable deviation from the ANOVA test assumptions is the non-homogeneity of variances, the test of variance was systematically performed. When the assumption of variance homogeneity was not met, the non-parametric Kruskal-Wallis test was applied.

Water and Sugar Content

After NMR experiments, the water content of all samples was estimated by measuring differences in weight after drying in an oven at 103°C for 24 hours. The mean water content estimated from five tomatoes was 93.6±0.7%, 95.3±0.4%, 95.9±0.4% and 96.1±0.3% for the core, placenta, outer pericarp and locular tissues, respectively. The ANOVA test indicated that in terms of water content, only the outer pericarp and the locular tissues were not different from each other.

Glucose and fructose were quantified using an enzymatic methods with kits for food analysis (Boehringer Mannheim Co., Mannhein, Germany) with an automatic analyser BM-

704 (Hitachi, Tokyo, Japan). The sugar content measurements were performed two days after the main MRI experiment on six samples from the placenta and pericarp and three samples from the locular tissue. The content of glucose were 17±3, 16±3 and 5±1 g/100 g of fresh weight for the placenta, outer pericarp and locular tissue, respectively. The content of fructose were 23±3, 17±3 and 9±1 g/100 g of fresh weight for the placenta, outer pericarp and locular tissue, respectively. The ANOVA test indicated that in terms of glucose content, the placenta and pericarp were different from the locular tissue, while in terms of fructose content all the tissues were different.

Macro Vision Imaging

Image acquisition

Four tomatoes were used for macro vision imaging. Samples were taken from the core, placenta and outer pericarp tissues. For each sample, 250 µm thick sections were obtained using a vibrating blade microtome (HM 650 V, Microm International GmbH, Walldrof, Germany). In addition, samples of locular tissue including seeds were taken and placed on a slide for direct observation. Tissues were observed using a macrovision system as described by Devaux et al [11] that included a CCD camera (Sony XC 8500 CE, Alliance Vision, Montélimar, France) fitted with a 50 mm lens (f 1:1.8 Nikon) and a 20 mm extension tube. Samples were back-lighted using a fiber-optic ring-light supplied by Polytec (Pantin, France). The camera and lens were adjusted to observe a 10.7 mm x 14.4 mm area. Images were digitized in 576 x 768 pixels of 18.6^2 µm². Gray levels were coded between 0 (black) and 255 (white). The lens aperture was set at 22. Two samples were taken per tissue and two images were recorded per sample. After preliminary observation, samples were placed in an ultrasonic bath (Ultrasons-Annemasse, Annemasse, France) for 15 s and in a dessicator connected to a pump for 30 s to remove any remaining air bubbles. Images were compared before and after degassing. Pericarp sections were placed under the camera to ensure that the cuticle was placed on the top of the images.

Image analysis

The aim was to extract quantitative information related to cell size. Image resolution did not allow segmentation of cells, and images were considered for visual texture according to both cell morphology and arrangement. Gray level granulometric methods were applied after image pre-treatment to extract global information concerning cell size distribution [11]. The method, developed using Matlab software and originating from mathematical morphology [12], consisted of the successive application of a basic procedure called “opening”. Only cells larger than the structuring element remain after an opening operation. The usual structuring elements are squares and oriented lines that are characterized by their side size, length and orientation, respectively. The proportion of variation of gray level of the image modified by opening depends on both the number of cells smaller than the structuring element and on the gray level values of the walls. A size distribution based on these gray level variations is obtained by applying a sequence of opening using structuring elements of increasing size.

In the case of pericarp images, both square and linear structuring elements were used. Linear structuring elements were chosen to analyze the length of cells perpendicular to the cuticle, while square elements were used to analyze the smallest cell dimension. In the case of the placenta and centre, no orientation was observed and only squared structuring elements were used. Thirty successive openings were applied, corresponding to structuring elements of lengths ranging from 5.25 µm to 1143.75 µm by increments of 37.5 µm. Gray level evolutions were normalized. No image analysis was applied on locular tissue images.

RESULTS

Magnetic Resonance Imaging

SE “morphological” images

An example of the SE “morphological” images is shown on Fig 1, including the tissue nomenclature as defined by Humle [9]. All tomatoes were composed of the following major regions: outer and radial pericarp, placenta, locular tissue and seeds. The tomato core was not distinguished from the placenta on these images. Seeds were clearly seen in locular

tissue as small regions of over-brightness. In SE “morphological” images ($TR<<T_1$ expected in vegetable tissues), signals arising from the pericarp and the placenta are less intense than signals originating from the locular tissue. This may indicate that higher T_1 relaxation times occur in the pericarp and placenta, but for reliable image interpretation T_1 and proton density maps have to be taken into account. Furthermore, as the TE of the imaging sequence was set at 15 ms, a T_2 effect on the signal intensity was also possible.

Relaxation times and proton density maps

Relaxation times and corresponding intensity maps calculated from the set of MSE and TOMROP images of the fruit in Fig. 1 are shown in Fig. 2. T_2 and T_1 relaxation maps reflect the morphological features of the tomato. Most of major regions of the tomato observed on the SE “morphological” images can be distinguished on both maps. Seeds did not appear in Fig. 2 because of the lower spatial resolution of MSE and TOMROP images compared to the SE images. On the other hand, core tissue, that is absent on SE images, can be distinguished on the T_2 map by careful observation. Both the T_2 and T_1 maps showed relatively short relaxation times in the placenta and core compared to the relaxation times observed in the pericarp and locular tissues. T_2 and T_1 increased gradually through the radial pericarp from the centre to the outer pericarp. This might be related to progressive changes in the structural aspects of these tissues. The locular tissue and pericarp were not clearly distinguished.

The average T_2 and T_1 values and standard deviations of voxels corresponding to different tissues of individual tomato fruits were extracted from the corresponding maps (Fig. 3). The progressive increase in T_2 and T_1 from the placenta to the outer pericarp is shown by the numerical values of relaxation parameters extracted from the images. It should be noted that the definition of tomato core tissue is not straightforward and its nature depends on where the imaged slice was selected. In fact, core tissue could correspond to collumela or to tissue with similar properties such as the placenta, which was the case for the majority of samples. In Fig. 3, T_1 and T_2 values of the third tomato indicate that its core was different from those of

other tomatoes and that it probably corresponded to the collumela. The mean relaxation times of the tissues calculated from all the tomatoes studied are given in Table 1.

T_2 and T_1 fitting errors were computed independently from the algorithms implemented on Scilab. For T_2 measurements, the mean fitting errors were 17 ms, 14 ms, 19 ms, 25 ms and 29 ms for the core, placenta, radial pericarp, outer pericarp and locular tissues, respectively. The errors were higher for T_1 adjustments, i. e. 76 ms, 67 ms, 78 ms, 83 ms and 98 ms for core, placenta, radial pericarp, outer pericarp and locular tissues, respectively. The large error of fitting for T_1 relaxation curves was due to a relatively lower signal to noise ratio for TOMROP images and to the use of a fitting model with higher degrees of freedom. In view of these results, relatively high values of standard deviations of mean T_2 and T_1 (Fig. 3), especially in the case of T_2 measurements where adjustment errors were small, can mainly be explained by variations between tomatoes.

The ANOVA test performed on mean values of T_2 and T_1 revealed that the variances of data in groups should be considered equal only when the core tissue was excluded. Therefore, the core tissue was not considered in these analyses. In the case of the T_2 measurements, all the tissues were statistically different. It was the same for the T_1 measurements, except that there was no statistical difference between the outer and the radial pericarp.

The relative mean average of M_0 (T_2) and $M_0(T_1)$ values for the different tissues are given in the Table 1. As for T_1 and T_2 analysis, the test of variance performed on $M_0(T_2)$ and $M_0(T_1)$ data revealed that the core tissue should be excluded from the analyses. The results of ANOVA for $M_0(T_2)$ indicated that all the tissues can be considered significantly different from each other, except for the outer pericarp and locular tissues which were not statistically different. In the case of $M_0(T_1)$, only the placenta can be considered different from other tissues. We assumed that M_0 obtained form the MSE and TOMROP images reflected the density of the water protons although other protons (fat, sugar) may have contributed to the signal intensity.

T_2 maps with variable echo time spacing

The MRI T_2-decay curves of the placenta tissue with various echo spacings (30, 50 and 90 ms) are shown on Fig. 4 a. For comparison purposes, a typical NMR T_2-decay curve, supposed to be free of any susceptibility effects because of the small echo spacing (1 ms), is superimposed on the MRI results. A distinct effect on the T_2 MRI measurements is observed due to an increase in the interecho spacing sequence. The T_2 of all tissues decreased for long interecho spacing, except the T_2 of the locular tissue (Fig. 4 b). The T_2 reduction was stronger for the core and the placenta than for the outer pericarp. The effects of the interecho spacing on the proton density maps were also observed, especially when interecho spacing was increased from 50 to 90 ms (not shown).

As a general rule, the dependence of T_2 on pulse spacing is related to the presence of the read gradients during the imaging experiment and/or to air bubbles in tissues. The contribution of the read gradient [13] to the observed T_2 was negligible in our experiment (the read gradient strength was 4.2 mT/m and the duration of the read gradient pulse was 30 μs) compared to high values for the relative T_2 loss. The dependence of T_2 on pulse spacing could thus be explained by diffusion of water molecules through internal magnetic field gradients generated caused by susceptibility inhomogeneities [14,15]. In view of the results of this section, it may be suggested that the placenta and core had significantly higher air bubble content than the outer pericarp and locular tissue.

.

Gradient echo images

An example of a gradient echo image of a tomato for TE_1= 9 ms and TE_2=40 ms is shown in Fig. 5. The contrast in the image with TE_1=9 ms is poor and tissues can be consequently hardly identified due to the relatively close T_1 relaxation times of different tissues and to the relatively short TE which did not allow T_2* contrast. In comparison, the contrast on the 40 ms echo time image is more pronounced. The distribution of T_2 relaxation times among different tissues had little impact on the contrast, which was verified on the SE images obtained by the MSE sequence at TE=30 and TE=60 (not shown). The contrast on the GE 40 ms echo time

images is thus due to the greater proportions of air in the placenta and core compared to other tissues. In order to evaluate the air bubble content, the 40 ms echo time images were divided by corresponding 9 ms echo time images and this relative signal was compared between different tissues. Fig. 6 shows that the relative signal intensity of the core and placenta tissues was lower than the relative signal from locular or pericarp tissues, indicating a greater amount of air in the first group of tissues. As the assumption of the variance homogeneity of the relative signal intensity data was not met the Kruskal-Wallis test was applied. The latter showed that all the tissues differed, except for the placenta and core that were not distinguished statistically.

Interpretation of contrast of "morphological" SE images

On the basis of the arguments reported above, it becomes obvious that the contrast in SE images (Fig. 1) depends on several parameters. In T_1 maps, T_1 increased gradually from placenta to locular tissue through the pericarp (see Fig. 3). The placenta should therefore have higher intensity than the locular tissue in T_1-weighted images. However, as shown in Fig. 1, the opposite occurred. This is partially explained by taking the proton density maps into account. The two processes work in opposite directions. The decreasing effect of the proton density on the signal intensity of the image exceeds the increasing effect of the T_1 value on the signal. This occurs because the proton density becomes the predominant contrast phenomenon when the relaxation times between the tissues are relatively close and much longer than TR. However, the difference in the signal intensity of the outer pericarp and the locular tissues cannot be explained by the differences in proton density. The lower signal of the pericarp compared to the locular tissue might be due to effects of air bubbles. This phenomenon was probably present in the placenta and the core, and emphasized contrast between these tissues and the locular tissue.

NMR Relaxometry

As expected, NMR relaxation measurements revealed a multi-component behavior of the signal. For all tomato tissues, the optimum adjustment of the T_2 relaxation signal was achieved by a four-exponential function (Table 1-a) independently of whether the adjustment method was discrete (Lavenberg-Marquardt algorithm) or continuous (MEM). In the majority of published studies [6,16-18], only three relaxation components were extracted for tissues of different plants and they were attributed to the cell wall, cytoplasm and vacuole compartments. Four relaxation components were found for apples [19], potatoes [20] and for tomatoes [6]. In the latter study the additional component relaxing with a smallest relaxation time was attributed to the non-exchangeable starch protons. According to these studies, it could be supposed that in our experiment component 1 corresponded to the non-exchangeable solute protons, and components 2, 3 and 4 to the water protons in the cell wall, cytoplasm and vacuole compartments, respectively. However, this hypothesis needs to be confirmed by further experiments. On the other hand, the optimum adjustment of the T_1 relaxation signal in the core and outer pericarp tissues of all tomatoes studied was obtained by a two-exponential function, with both the discrete and the continuous methods. This difference between numbers of T_1 and T_2 components was probably due to similar values of T_1 for the first and second T_2-components, and to similar values of T_1 for the third and forth T_2-components. This hypothesis is supported by comparing the relative signal intensity of corresponding T_2 and T_1 components.

The results of the T_1 measurements for the placenta were judged aberrant and they are therefore not reported. This can be explained by the sedimentation of placenta tissue which appeared to be more sensitive to this phenomenon than the other tissues studied. The T_2 measurements were not affected by sedimentation because they were performed systematically before T_1 measurements and because of their relatively short acquisition time.

Comparison of the Results of NMR and MRI Measurements

In order to make possible the comparison between NMR and MRI results, we considered that the MRI T_2 and T_1 correspond to weighted averages of the corresponding peaks found in

NMR experiments. The weighted averages NMR T_2 (T_2-wa) and (T_1-wa) values are presented in the last columns of the Table 1 a and b. In the case of T_2, the first components of the NMR signal were not taken into account because of their low relaxation times and low signal intensities. In fact, in MRI MSE experiments the components with T_2 of about 30 ms or less were ignored as the first echo time was 30 ms.

The ANOVA test applied to T_2-wa showed that two groups of tissue could be distinguished on the basis of T_2 measurements. The core and placenta had significantly shorter relaxation times than the outer pericarp, in agreement with the MRI results. However, contrary to MRI, NMR did not distinguish the core of the placenta. As expected, the T_2-wa of the placenta and pericarp measured by NMR was higher than the T_2 measured by MRI, indicating that the effects of susceptibility were probably present in the MRI measurements. The NMR T_1-wa of the core was lower than that of the locular tissue, and the ANOVA test confirmed their statistical difference. However, although the NMR experiments were performed at a higher magnetic field than the MRI measurements, the weighted NMR average T_1 was lower than the T_1 measured by MRI for all tissues. The differences between the absolute values of MRI relaxation times and those of weighted NMR averages were probably due to differences in measurement techniques and to the correcting method for the T_1 computing from the TOMROP sequence.

Macro Vision Imaging

Macro vision images of outer pericarp, placenta and core tissues before and after degassing are presented in Fig. 7. An additional image of locular tissue including seeds is also given. The presence of gas is demonstrated by regions or points of over-brightness in the images acquired before degassing. The presence of air bubbles results in considerable light diffusion and saturation of image intensity. Figure 7 shows that this over-brightness was partially or entirely removed after degassing the samples, making the cellular structure of the samples clearly visible. Comparison of images before and after degassing did not make it possible to quantify air in tissues, but it clearly showed that the placenta and core tissues

were significantly richer in air than the outer pericarp tissue. In addition, it was much more difficult to remove air bubbles from these two tissues than from pericarp tissues.

The results from the granulometric study showed that cells of the placenta and the core tissues were of similar size (about 100 μm, referring to the size of the squared structuring element used in image analysis) and no trend in cell distribution was observed. In contrast, the pericarp tissue had larger cells and specific cell distributions. The smallest dimension of cells was around 200 μm as revealed by granulometry using a squared structuring element, while the length perpendicular to the cuticle was much greater, with sizes ranging up to 600-700 μm. The heterogeneity of cell length was demonstrated by the wide size variations observed using linear structuring elements.

DISCUSION AND CONCLUSION

This study indicates that an imaging sequence that results in contrast of a combination of parameters (M_0, T_1, T_2) could not be used as a correct and single interpretation of the structural aspects of fruit. The example of SE images (Fig. 1) showed that interpretation became very complicated when different processes work in opposite directions. Measurement of the distribution of individual physical parameters such as proton density and T_1 and T_2 was thus a more reliable method for plant investigations. However, even at a low field, the parameters of the multi-echo sequences must be chosen carefully. Susceptibility inhomogeneities appeared to influence T_2 and M_0 measurements when long inter-echo spacing was employed in a multi-echo sequence. These effects were higher on T_2 maps than on calculated intensity images, but the results indicated that the intensity images can be considered as proton density maps only for relatively short echo times.

We showed in this study by both MRI and NMR measurements that the core and placenta tissues of the tomato are characterized by lower relaxation times than other tissues. This is in agreement with the results of the cell size estimations from macro vision images, which demonstrated that cells of the outer pericarp were significantly larger then cells of the core and placenta tissues. The general rule states that for vacuolized plant cells, like those of the

tomato, the smaller the cell size, the shorter its T_2 value [8]. Further, the results of $M_0(T_2)$ mapping agree with the results obtained from the classical water content measurements, revealed that the water content is correlated to the relaxation times of tissues. Finally, the concentration of the sugars was the highest within the placenta, followed by the outer pericarp and the locular tissue which is correlated to theirs relaxation times. However, it is hard to separate the effects of the cell size from the water and sugar contents on the relaxation times since a positive correlation was observed between all of these physiological parameters.

The MRI relaxation maps are derived from a lower echo number compared to the NMR method and echoes are acquired with relatively wide time spacing. Thus MRI data often do not make it possible to resolve contributions from the different sub-cellular water compartments and they are contaminated by susceptibility effects. In addition, the maximum number of consecutive echoes in our multi-echo imaging sequences was limited to 32. For products with long T_1 and T_2 relaxation times like tomatoes, the inter-echo spacing has to be long to permit acquisition of a significant part of the relaxation curve, especially when it needs to be constant. However, the non-invasive character of the MRI permitted successful investigation of all the types of tomato fruit tissues, which was not the case for NMR Relaxometry that was limited by imprecise sampling and sedimentation of sampled tissues. MRI was also shown to be more sensitive to tissue discrimination than NMR.

Different quantities of air bubbles throughout the tissues were demonstrated in two different ways. We used the relative signal deducted from gradient echo images with different echo times. These ratio images did not allow rigorous calculation of T_2^* because the gradient echo signal decreases exponentially as a function of TE only for a relatively low volume fraction of the susceptibility source and for a limited range of echo times [21]. However, ratio images provided a good means for evaluating air distribution and showed that placenta and core tissues had a higher air bubble content than other tissues. These results agreed with the results of the MSE experiment with various echo spacing. Finally, the results were consistent with macro vision images in which air bubbles in tissues were clearly visualized.

This study showed that quantitative MRI at low field was able to distinguish different tissue types in tomato fruit. The information about the distribution of T_2 and T_1 relaxation times and air bubble distribution in the tomato provides a reference results for future development of relaxation time or susceptibility -weighted pulse sequences either to enhance or suppress the contrast between different components of tomato fruit. The results from this study contribute to the understanding of the relationship between physiological and NMR parameters which is necessary for further investigations of tomato during growing or ripening. These aspects will be investigate in our further study.

Acknowledgment: The authors wish to thank CTIFL and especially Mr. Letard for their collaboration. We also thank Maryse Reich and Sylvie Bureau du "Plateau technique de mesure et de caractérisation de la qualité" UR SQPOV, INRA, Avignon and Mr. Taverson for their contribution to the experimental work.

REFERENCES

1. Hills BP, Clark CJ. Quality assessment of horticultural products by NMR. Annual Reports on NMR Spectroscopy 2003;50:75-120.
2. Saltveit ME. Determining Tomato Fruit Maturity with Nondestructive In Vivo Nuclear Magnetic Resonance Imaging. Postharvest Biol Technol 1991;1:153-159.
3. Ishida N, Kobayashi T, Koizumi M, Kano H. 1H-NMR Imaging of Tomato Fruits. Agric Biol Chem 1989;53(9):2363-2367.
4. Iwahashi Y, Horigane AK, Yoza K, Nagata T, Hosoda H. The study of heat stress in tomato fruits by NMR microimaging. Magnetic Resonance Imaging 1999;17(5):767-772.
5. Gonzalez JJ, McCarthy K, McCarthy MJ. MRI Method to Evaluate Internal Structural Changes of Tomato during Compression. Journal of Texture Studies 1998;29:537-551.

6. Duval F, Cambert M, Mariette F. NMR study of tomato pericarp tissue by spin-spin relaxation and water self-diffusion. Appl Magn Reson 2005;28(1-2):29-40.
7. Pickup S, Wood AKW, Kundel HL. A Novel Method for Analysis of TOMROP Data. J Magn Reson Imaging 2004;19:508-512.
8. Edzes HT, van Dusschoten D, Van As H. Quantitative T2 Imaging of Plant Tissues By Means Of Multi-Echo MRI Microscopy. Magn Reson Imaging 1998;16(2):185-196.
9. Humle AC. The Biochemistry of Fruits and their Products. London and New York: Academic Press 1971.
10. Mariette F, Guillement JP, Tellier C, Marchal P. Continuous Relaxation Time Distribution Decomposition by MEM. In: N. RD, editor. Signal Treatment and Signal Analysis in NMR. Paris: Elsevier; 1996. p 218-234.
11. Devaux M-F, Bouchet B, Legland D, Guillon F, Lahaye M. Macro-vision and grey level granulometry for quantification of tomato pericarp structure. Postharvest Biology and Technology 2008;47(2):199-209.
12. Soille P. Morphological Image Analysis: Principles and Applications Berlin: Springer-Verlag; 2003.
13. Donker HCW, VanAs H, Edzes HT, Jans AWH. NMR imaging of white button mushroom (Agaricus bisporis) at various magnetic fields. Magnetic Resonance Imaging 1996;14(10):1205-1215.
14. Duce SL, Carpenter TA, Hall LD, Hills BP. An Investigation of the Origins of Contrast in NMR Spin Echo Images of Plant Tissue. Magn Reson Imaging 1992;10:289-297.
15. Van As H. Intact plant MRI for the study of cell water relations, membrane permeability, cell-to-cell and long distance water transport. Journal of Experimental Botany 2007;58(4):743-756.
16. Snaar JEM, Van As H. Probing Water Compartements and Membrane Permeability in Plant Cells by H NMR Relaxation Measurements. Biophysical Journal 1992;63:1654-1658.

17. Van Dusschoten D, De Jager PA, Van As H. Extracting diffusion constants from echo-time-dependent PFG NMR data using relaxation-time information. J Magn Reson Ser A 1995;116(1):22-28.
18. Snaar JEM, Van As H. A method for the simultaneous measurement of NMR spin-lattice and spin-spin relaxation times in compartmentalized systems. Journal of Magnetic Resonance 1992;99:139-148.
19. Sibgatullin TA, Anisimov AV, de Jager PA, Vergeldt FJ, Gerkema E, Van As H. Analysis of diffusion and relaxation behavior of water in apple parenchymal cells. Biofizika 2007;52(2):268-276.
20. Mariette F, Brannelec C, Vitrac O, Bohuon P. Effet du procédé de friture sur la répartition et l'état de l'eau mesurée par RMN et IRM. 1999; Nantes. Edition Tec & Doc. p 411-416.
21. Cheng Y-CN, Haacke EM, Yu Y-J. An exact form for the magnetic field density of states for a dipole. Magnetic Resonance Imaging 2001;19(7):1017-1023.

Table 1 : a - The mean values of MRI (T_2 and $M_0(T_2)$) and NMR (multi component T_2, corresponding relative signal intensities and weighted T_2 average (T_2-wa)) measurements for the different tomato tissues. b – Corresponding results of T1 measurements

Fig 1: SE MRI image of the median equatorial plane of tomato with tissue annotation.

Fig. 2 : T2 (a) map and corresponding calculated intensity image $M_0(T_2)$ (b) of tomato. T_1 (c) and corresponding calculated intensity image $M_0(T_1)$ (d) of the same fruit.

Fig. 3 : Mean T_2 (a) and T_1 (b) values and standard deviations of tomato tissues. Bars correspond to different tomatoes. Tomatoes presented on the T_1 histogram correspond to the first three tomatoes presented on the T_2 histogram.

Fig. 4 : a - Typical MRI T_2-decay curves of mean signal of the placenta tissue with inter-echo spacing of: ■ - 30 ms, ▲ - 50 ms and ● - 90 ms with corresponding fits (dashed lines). Solid line corresponds to RMN data obtained on the placental tissue of another tomato. b - T2 of different tissues extracted from MRI maps acquired with various inter-echo spacing (● - placenta; ■ - core; ◇ - radial pericarp; □ - outer pericarp; ◆ - locular tissue)

Fig. 5: Normalised gradient echo images of a tomato for TE of 9 ms (a) and 40 ms (b).

Fig. 6 : Mean relative signals of tomato tissues obtained by division of the 40 ms echo time GE images by corresponding 9 ms echo time images. The errors correspond to the standard deviation of the mean relative signal.

Fig 7 : Macro vision images of (a) outer pericarp, (b) placenta and (c) core before (left column) and after (right column) degasifying. Image of locular tissue (d). The images were coded between 0 (black) and 255 (white) and their size were 10.7 mm X 14.4.

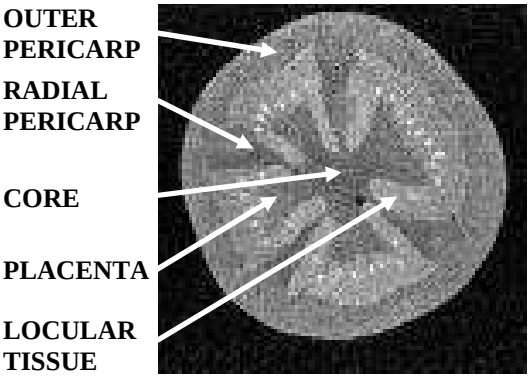
OUTER PERICARP
RADIAL PERICARP
CORE
PLACENTA
LOCULAR TISSUE

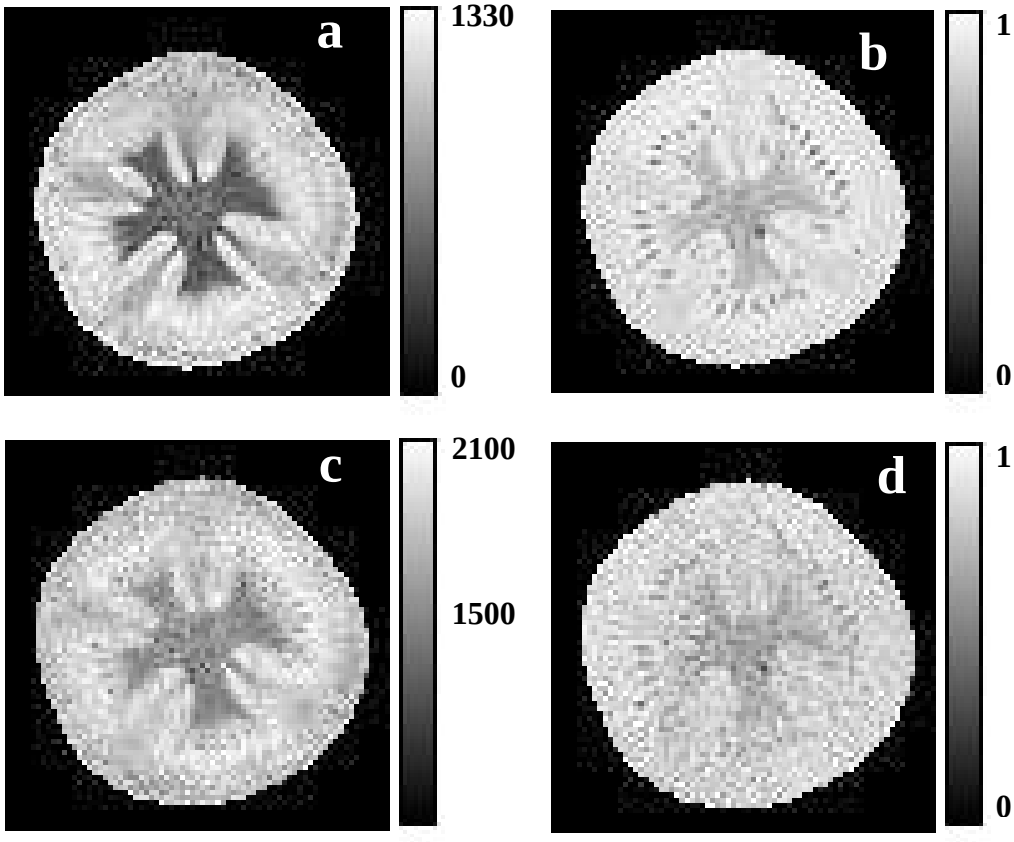
a
1330
0
b
1
0
c
2100
1500
d
1
0

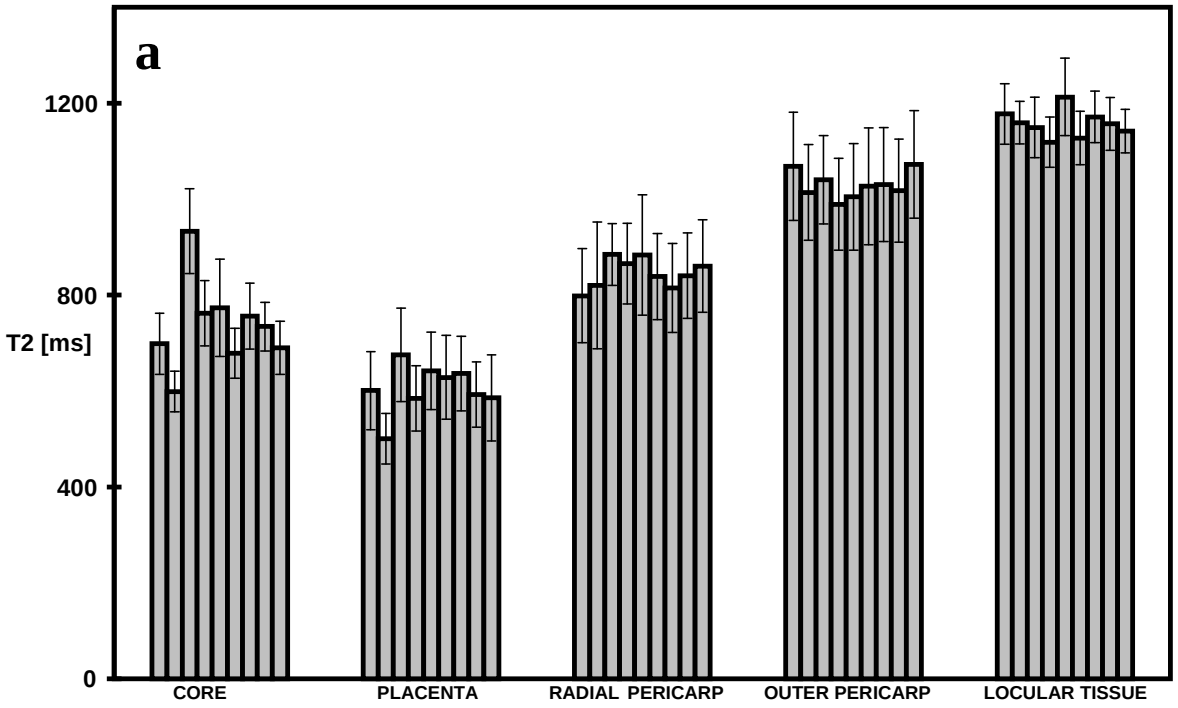
a
1200
800
T2 [ms]
400
0
CORE
PLACENTA
RADIAL PERICARP
OUTER PERICARP
LOCULAR TISSUE

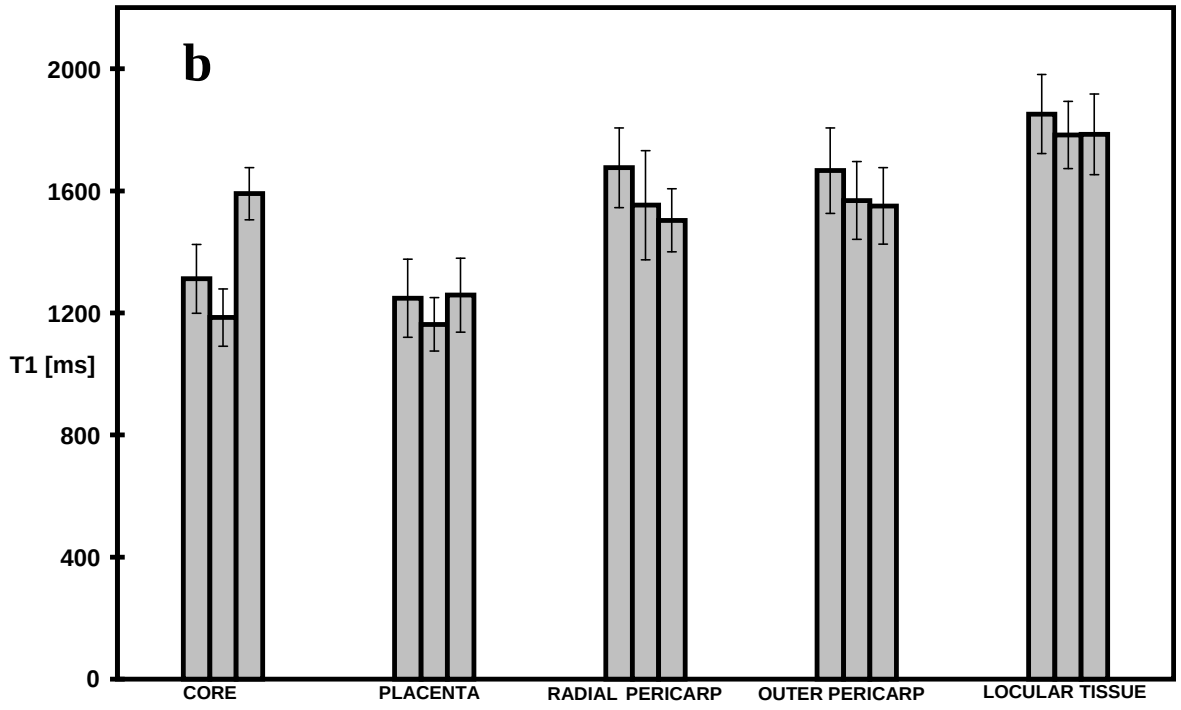
b
2000
1600
1200
T1 [ms]
800
400
0
CORE
PLACENTA
RADIAL PERICARP
OUTER PERICARP
LOCULAR TISSUE

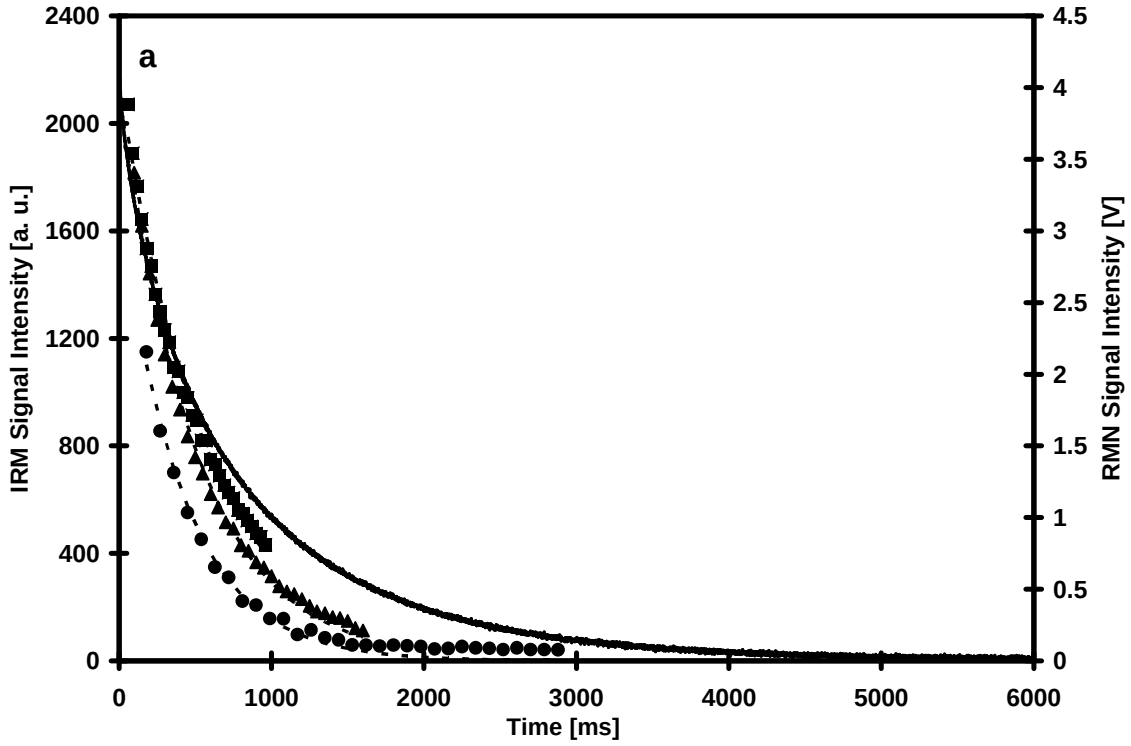
a
IRM Signal Intensity [a. u.]
RMN Signal Intensity [V]
Time [ms]
2400
2000
1600
1200
800
400
0
4.5
4
3.5
3
2.5
2
1.5
1
0.5
0
0
1000
2000
3000
4000
5000
6000

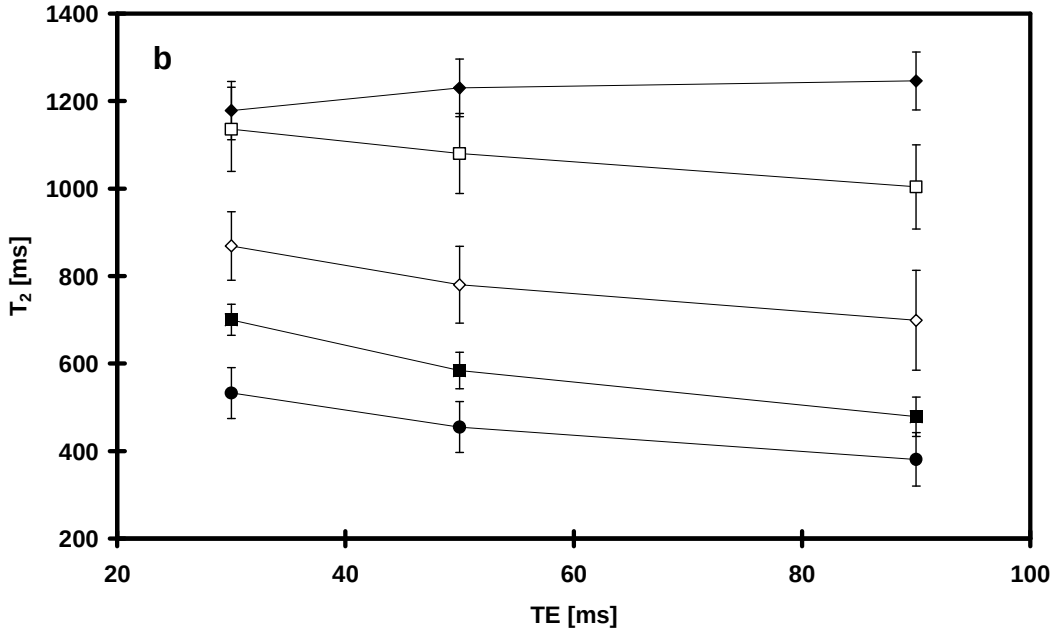
b
T2 [ms]
TE [ms]
1400
1200
1000
800
600
400
200
20
40
60
80
100

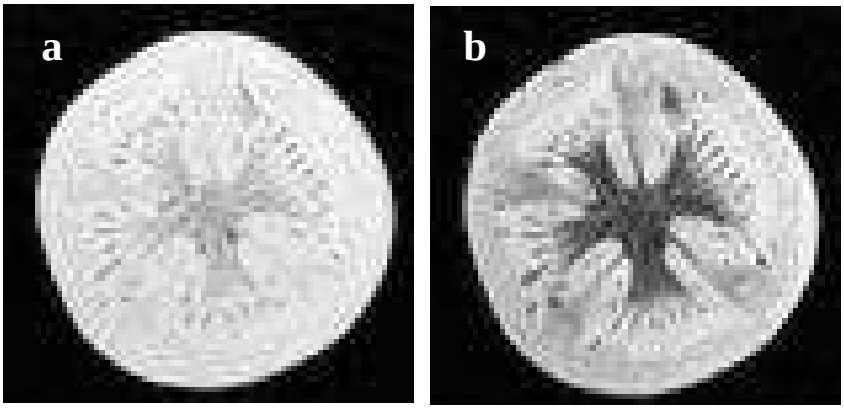
a
b

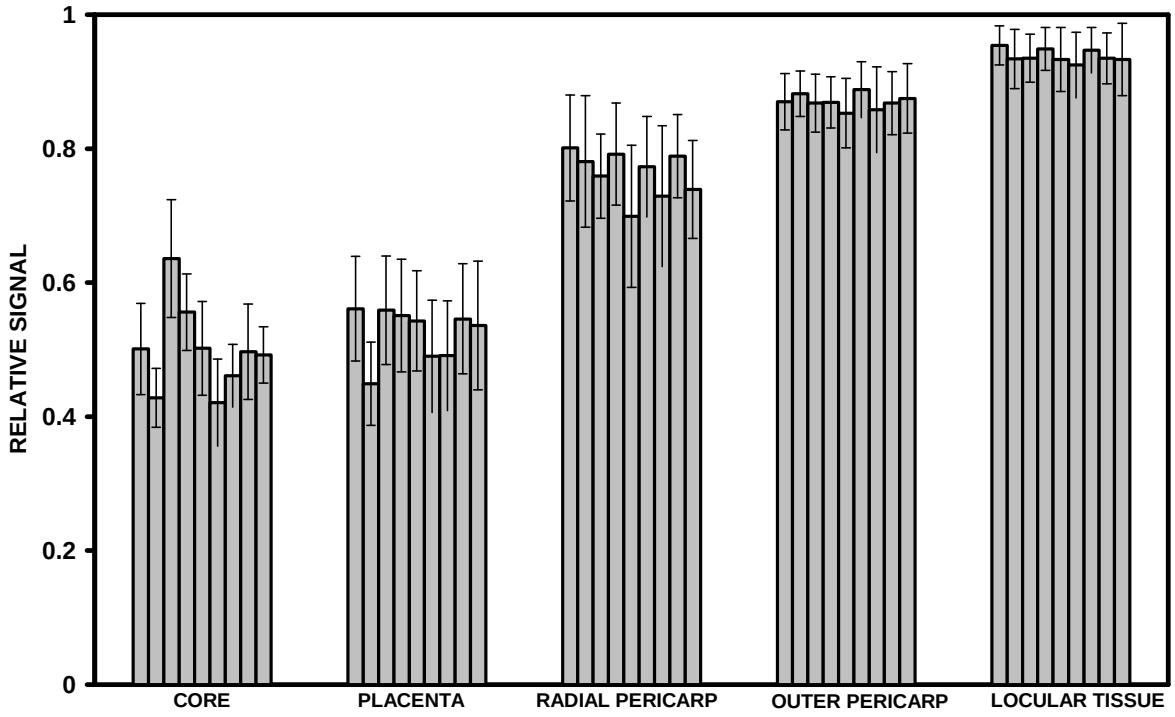
RELATIVE SIGNAL
1
0.8
0.6
0.4
0.2
0
CORE
PLACENTA
RADIAL PERICARP
OUTER PERICARP
LOCULAR TISSUE

BEFORE DEGAZIFYNG **AFTER DEGAZIFYNG**

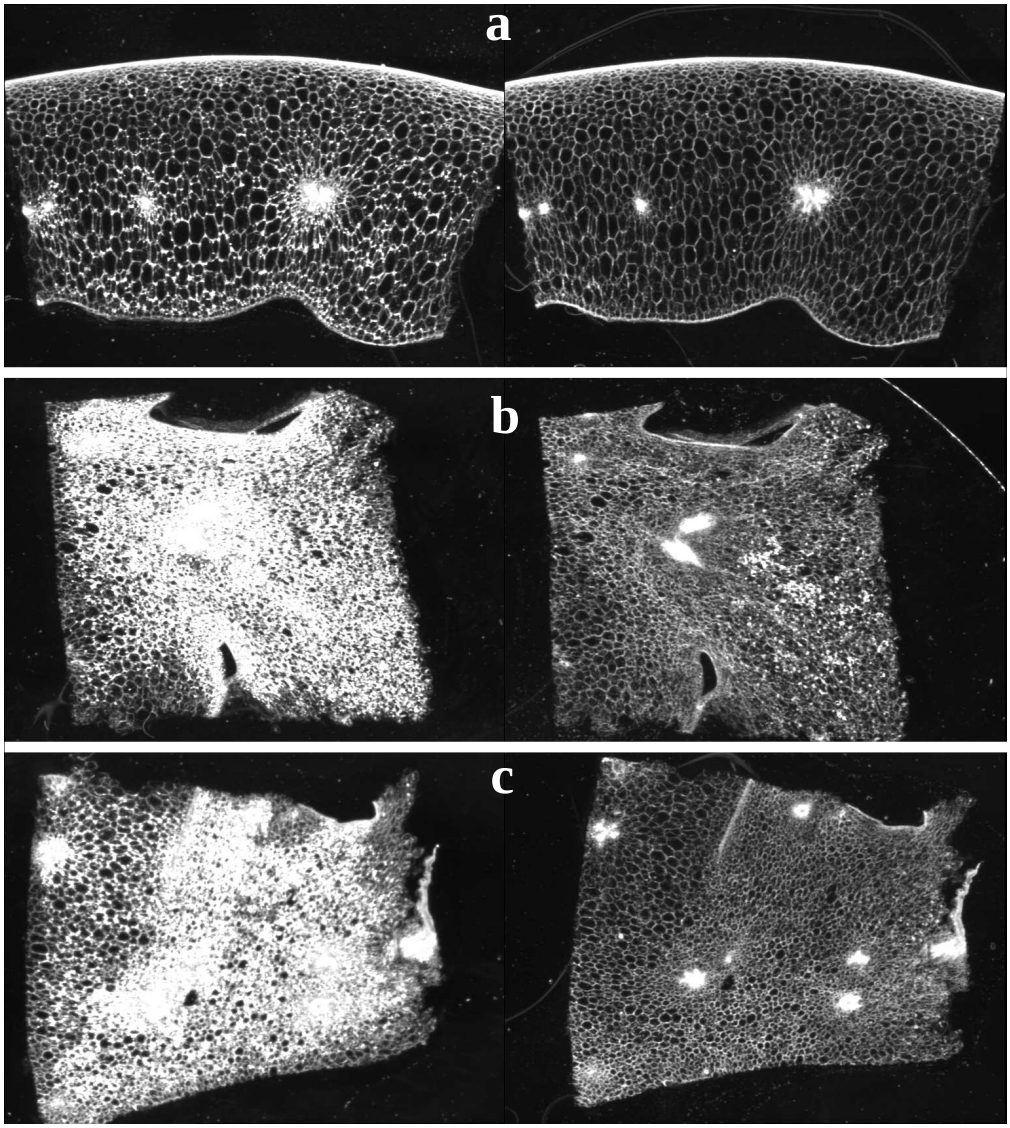

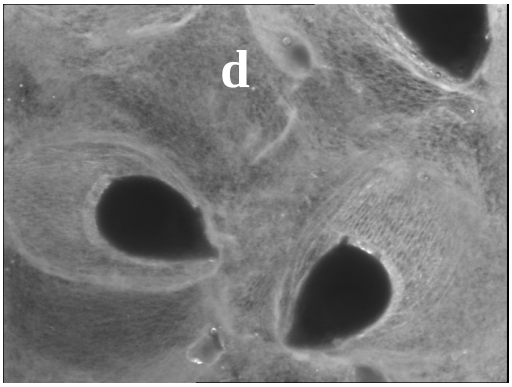

a	MRI		NMR								
	T_2 [ms]	$M_0(T_2)$ [a.u.]	T_{21} [ms]	I_{01} [%]	T_{22} [ms]	I_{02} [%]	T_{23} [ms]	I_{03} [%]	T_{24} [ms]	I_{04} [%]	T_2-wa
CORE	712±58	0.71±0.04	18±3	9±1	99±11	21±5	387±48	34±6	1185±172	37±3	654±152
PLACENTA	605±50	0.73±0.02	19±3	4±0	129±21	10±1	414±58	30±4	930±78	56±5	686±44
RADIAL PERICARP	845±31	0.82±0.02	***	***	***	***	***	***	***	***	***
OUTER PERICARP	1029±28	0.85±0.02	31±9	6±2	150±39	9±2	605±122	23±4	1527±120	62±6	1168±66
LOCULAR TISSUE	1157±28	0.85±0.02	***	***	***	***	***	***	***	***	***

b	MRI		NMR				
	T_1 [ms]	$M_0(T_1)$ [a.u.]	T_{11} [ms]	I_{11} [%]	T_{12} [ms]	I_{01} [%]	T_1-wa
CORE	1362±90	0.69 ±0.05	338±41	36±5	1280±161	64±5	942±158
PLACENTA	1223±50	072. ±0.03	***	***	***	***	***
RADIAL PERICARP	1579±89	0.80 ±0.01	***	***	***	***	***
OUTER PERICARP	1595±62	0.83 ±0.01	459±50	20±4	1692±112	80±4	1440±87
LOCULAR TISSUE	1807±39	0.80 ±0.02	***	***	***	***	***